Peer-reviewed version available at Appl. Sci. 2018, 8, 2689; doi:10.3390/app8122689

Article

Simulating the Impact of the Internal Structure of Phytoplankton on the Bulk Particulate Backscattering Ratio using a Two-Layered Spherical Geometry for Cells

Lucile Duforêt-Gaurier [1]*, David Dessailly [1], William Moutier [2] and Hubert Loisel [1]

[1] Univ. Littoral Cote d'Opale, Univ. Lille, CNRS, UMR 8187, LOG, Laboratoire d'Océanologie et de Géosciences, F 62930 Wimereux, France; lucile.duforet@univ-littoral.fr; david.dessailly@univ-littoral.fr; hubert.loisel@univ-littoral.fr

[2] Royal Meteorological Institute of Belgium, B-1180 Brussels, Belgium; william.moutier@gmail.com

* Correspondence: lucile.duforet@univ-littoral.fr; Tel.: +33-321996421

Abstract: The bulk backscattering ratio ($\tilde{b_{bp}}$) is commonly used as a descriptor of the bulk real refractive index of the particulate assemblage in natural waters. Based on numerical simulations, we analyze the impact of heterogeneity of phytoplankton cells on $\tilde{b_{bp}}$. $\tilde{b_{bp}}$ is modeled considering viruses, heterotrophic bacteria, phytoplankton, detritus, and minerals. Three study cases are defined according to the relative abundance of these different components. Two study cases represent typical situations in open ocean, outside (No-B/No-M) and inside bloom (B/No-M). The third study case is typical of coastal waters with the presence of minerals. Phytoplankton cells are modeled by a two-layered spherical geometry representing a chloroplast surrounding the cytoplasm. The $\tilde{b_{bp}}$ values are higher when heterogeneity is considered because the contribution of coated spheres to backscattering is higher than homogeneous spheres. The impact of heterogeneity is however strongly conditioned by the hyperbolic slope ξ of the particle size distribution. Even if the relative concentration of phytoplankton is small (<1%), $\tilde{b_{bp}}$ increases by about 60% (for $\xi = 4.3$ and for the No-B/No-M water body), when the heterogeneity is taken into account, in comparison with a particulate population only composed by homogeneous spheres. As expected, heterogeneity has a much smaller impact (about 5% for $\xi = 4.3$) on $\tilde{b_{bp}}$ when minerals are added.

Keywords: Ocean optics; backscattering ratio; phytoplankton, coated-sphere model, bulk refractive index, seawater component

1. Introduction

Seawater constituents (pure water molecules, suspended particles, dissolved substances, and air bubbles) impact the propagation of light through absorption and scattering processes. In natural waters, suspended particulate matter is mostly composed of phytoplankton, heterotrophic organisms, viruses, biogenic detritus, and mineral particles. Absorbing and scattering characteristics of water constituents are described by the Inherent Optical Properties (IOPs) [1] which do not depend on the radiance distribution but on the concentration, chemical composition of dissolved organic matter, and the concentration, size distribution and chemical composition of particulate matter. All IOPs can be defined from the absorption coefficient, a, and the volume scattering function, β. For instance, the scattering, b, and backscattering, b_b, coefficients are obtained from the integration of β over the whole direction, and only in the backward direction, respectively.

Thanks to the availability of commercial optical backscattering sensors and flow-through attenuation and absorption meters, in situ measurements of bulk IOPs are now routinely performed for more than two decades. While these measurements allow a better description and knowledge

Peer-reviewed version available at Appl. Sci. 2018, 8, 2689; doi:10.3390/app8122689

of the IOPs variability in natural waters to be achieved, they can also be used as pertinent proxies of the bulk particulate matter. For instance, the slope of the particulate beam attenuation coefficient, c_p, is tightly linked to the slope of the particulate size distribution (PSD), ξ, assuming a Junge-type distribution [2–4]. This latter coefficient, combined with the particulate backscattering to scattering ratio, b_{bp}/b_p, where b_{bp} and b_p are respectively the particulate backscattering and scattering coefficients, are the two required input parameters to assess the bulk real refractive index of marine particles, $\tilde{n_r}$, from theoretical simulations. Based on the Lorentz-Mie theory calculations that assumes marine particles as homogeneous spheres, an analytical relationship between b_{bp}/b_p, ξ and n_r was generated [5]. This later equation is widely used to describe, from in situ b_{bp}, b_p, and c_p measurements, the variability of the chemical nature (i.e. refractive index) of the bulk particulate matter in oceanic and coastal environments [6–10].

For the past few years, many theoretical or experimental studies, mainly dedicated to phytoplankton, showed that while the absorption, attenuation and total scattering of algal cells are correctly described using the homogeneous sphere model, this latter is less appropriate to simulate the backscattering. Indeed, the phytoplankton heterogeneity and inner complexity (gas vacuoles, chloroplast, silica wall, etc.) explain why the measured backscattering signal is higher than predicted by the Lorentz-Mie theory [11–18]. The underestimation of b_{bp} by homogeneous spheres may explain partly the backscattering enigma that lies in the fact that in situ observations of backscattering are significantly higher than theoretical simulations [19,20].

In this paper, we will study the impact of particle heterogeneity on the bulk backscattering ratio for realistic combinations of optically significant constituents of three different natural water bodies. Typical phytoplankton bloom and no blooms conditions, as defined in Stramski and Kiefer [21], will first be examined. Then, the last study case will account for the presence of mineral particles which have a great effect on the scattering properties. For that purpose, and because the bulk scattering (b) and backscattering (b_b) coefficients of a water body result from additive contributions of all individual constituents that scatter light, we will consider different sub-populations of marine particles and a more realistic model (compared to an homogeneous sphere) for phytoplankton cells. Bernard et al. [22] highlighted that the real refractive index of the chloroplast and the relative volume of the chloroplast are key parameters impacting the backward efficiency. This was recently confirmed by two recent studies where in situ measurements of the scattering on phytoplankton cultures were well reproduced by the two-sphere model [13,14]. For these reasons, phytoplankton optical properties will be simulated considering a two-layered sphere model. The size range of the different considered particles (virus, bacteria, phytoplankton, and detritus), as well as their real and imaginary refractive index values are defined from literature [19,23].

In order to establish the foundations of the present study, the different theoretical considerations, as well as the two different numerical codes used for the calculations, are first presented. Then, we will detail the different sub-populations of particles and their associated size distribution, refractive indices, and internal structures used to simulate their optical properties. The impact of the heterogeneity will then be discussed for the three realistic water bodies as mentioned previously.

2. Theoretical considerations

2.1. Polydisperse backscattering cross section

Light scattering is produced by the presence of an object (such as a particle) with a refractive index different from that of the surrounding medium. The refractive index is expressed in complex form as $n(\lambda) = n_r(\lambda) + i\ n_i(\lambda)$, where λ is the wavelength of the radiation in the vacuum in units of nm. The real part determines the phase velocity of the propagating wave and the imaginary part accounts for the absorption. The single scattering process by a particle is described by the scattering

Peer-reviewed version available at Appl. Sci. 2018, 8, 2689; doi:10.3390/app8122689

Table 1. Summary of the seawater constituents

Component	Sphere model	D_{min}-D_{max} (μm)	n_r	n_i
Viruses	homogeneous	0.03-0.2	1.05	0
Heterotrophic bacteria	homogeneous	0.2-2	1.05	$1.0.10^{-4}$
Phytoplankton cells	two-layered	0.2-40	1.044*	1.5×10^{-3}*
Organic detritus	homogeneous	0.05-500	1.04	$2.3.10^{-5}$
Minerals	homogeneous	0.05-500	1.18	$1.0.10^{-4}$

* *the values represent the equivalent refractive indices (Equation 11). The refractive indices of the chloroplast and cytoplast are described in Table 2. λ = 532 nm.*

cross section $C_{sca}(D,\lambda)$ (units m^2) and the normalized phase function $F(D,\theta,\lambda)$ [24] as defined by Equation (1).

$$\int_0^{\pi} F(D,\lambda,\theta)\, sin\theta\, d\theta = 2 \tag{1}$$

As particles are here assumed to be spherical, the scattering function only depends on the particle diameter D, the zenithal angle θ, and the wavelength λ. In the following, λ is omitted for clarity. To account for polydisperse assemblages, the Particulate Size Distribution (PSD) (units, number of particles per unit volume) is defined. For the present study, we adopt a power-law PSD (also named the Junge-like PSD) which is commonly used to represent the size distribution of marine particles in natural waters [5], [25,26]. The ensemble-average phase function is:

$$F(\theta) = \int_{D_{min}}^{D_{max}} F(D,\theta) \times A\, D^{-\xi} dD \tag{2}$$

where D_{min} and D_{max} define the diameter range, $AD^{-\xi}$ is the number of particles per unit volume (part/m^3) in the size range dD, and ξ is the hyperbolic slope. As in many theoretical studies, the PSD is normalized such that the integral over the size range is unity. It results that $F(\theta)$ represents the average phase function per particle. Equation (2) can be written for the scattering cross section replacing $F(D,\theta)$ by $C_{sca}(D)$ and $F(\theta)$ by C_{sca}. The backscattering cross section of the polydisperse assemblage is defined as:

$$C_{sca}^{bb} = \frac{C_{sca}}{2} \int_{\pi/2}^{\pi} F(\theta)\, sin\theta\, d\theta \tag{3}$$

It can be easily seen from Eqs. (1-3) that the integration of $F(\theta)$ between 0 and π gives C_{sca}, the scattering cross section of the polydisperse population.

2.2. The bulk backscattering ratio

Marine particles are lumped into five different compartments: viruses (VIR), heterotrophic bacteria (BAC), phytoplankton (PHY), detritus (DET) and minerals (MIN). Table 1 displays the size ranges and the refractive indices of the different components as defined by previous studies [19], [23], [21]. The ensemble-average $F^j(\theta)$, C_{sca}^j, and $C_{sca}^{bb,j}$ are computed from Equations (1-3) for each component j.

The total normalized phase function and total scattering cross section of the water body are obtained as follows:

$$F^{tot}(\theta) = \frac{\sum_{j=1}^{5} N^j C_{sca}^j F^j(\theta)}{\sum_{j=1}^{5} N^j C_{sca}^j} \tag{4}$$

$$C_{sca}^{bb,tot} = \sum_{j=1}^{5} N^j C_{sca}^{bb,j}. \quad (5)$$

where N^j is the relative concentration of the considered component. C_{sca}^{tot} is defined by replacing $C_{sca}^{bb,j}$ by C_{sca}^{j} in Equation (5).

The total (i.e., bulk) backscattering coefficient (b_{bp}) (units m^{-1}) of the water body is the sum of the relevant b_{bp}^{j} associated with the jth group. b_{bp}^{j} is equal to the polydisperse $C_{Sca}^{bb,j}$ weighted by the particle concentration into the jth group:

$$b_{bp} = \sum_{j=1}^{5} b_{bp}^{j} = N_{TOT} \times C_{sca}^{bb,tot} \quad (6)$$

with N_{TOT} the total concentration (part/m^3) in the water body. Equally, b_p is defined from Equation (6) by replacing b_{bp} by b_p and $C_{sca}^{bb,tot}$ by C_{sca}^{tot}. The bulk backscattering ratio $\tilde{b_{bp}}$ is the dimensionless ratio:

$$\tilde{b_{bp}} = \frac{b_{bp}}{b_p}, \quad (7)$$

In this study, we will use the bulk real particulate refractive index ($\tilde{n_r}$), which reproduces the bulk scattering properties of a water body. It represents the mean refractive index weighted by the scattering cross sections of all the particles:

$$\tilde{n_r} = \frac{\sum_{j=1}^{5} n_r^j \times N^j C_{sca}^j}{\sum_{j=1}^{5} N^j C_{sca}^j} \quad (8)$$

Equivalently, the bulk imaginary refractive index ($\tilde{n_i}$) is defined as follows:

$$\tilde{n_i} = \frac{\sum_{j=1}^{5} n_i^j \times N^j C_{abs}^j}{\sum_{j=1}^{5} N^j C_{abs}^j} \quad (9)$$

with C_{abs}^{j} the absorption cross section of particles.

2.3. The scattering coefficient as measured by in situ transmissiometers

In field measurements, b_p is derived from the total absorption and attenuation coefficients (a and c, respectively) as measured by transmissiometers such as, for example, WETLabs C-Star or ac9 and its later variants. Any detector has a finite field of view (FOV). It results that transmissiometers are defined by their acceptance angle $\theta_{acceptance}$, which differs from 0^o. If we want to compare, in a future study, our theoretical results to available in-situ measurements, b_p must be derived from C_{sca}, rebuilt from the phase function integrated between $\theta_{acceptance}$ and π instead of 0 and π [27]. To make a distinction, when C_{sca} is calculated by integrating the scattering function between $\theta_{acceptance}$ and π, the terminology $C_{sca}^{\theta_a}$, $b_p^{\theta_a}$ and $\widetilde{b_{bp}^{\theta_a}}$ (= $b_{bp}/b_p^{\theta_a}$) will be used. As in Twardowski et al. [5], we set the acceptance angle to 1^o, which is consistent with acceptance angles of commercially-available instruments as the WETLabs C-Star (1.2^o) or WETLabs ac9 (0.93^o) ([27] and references therein).

Table 2. Refractive index ($n_r(chl) + i\, n_i(chl)$) of the chloroplast for two morphological models. The refractive index of the cytoplast is constant (1.02+i 1.3357×10^{-4}). The equivalent refractive index of the cell is 1.044+i 1.5×10^{-3}.

Model* (%cyt-%chl)	80%-20%	70%-30%
n_r	1.14	1.10
n_i	6.9657×10^{-3}	4.6883×10^{-3}

* *The percentages represent the relative proportions of the cytoplasm and chloroplast in volume*

3. Numerical modeling of the marine particle scattering

The Meerhoff Mie program, version 3.0 [28] and the Scattnlay code [29,30] are used to simulate the scattering and absorbing properties of homogeneous and multi-layered spheres, respectively. Radiative transfer computations were carried out, given the wavelength of the incident radiation equal to 532 nm and the refractive index of water equal to 1.34. The Meerhoff Mie program allows simulations of a polydisperse ensemble of spheres with a large choice of PSD. The ouputs are the ensemble-average quantities per particle $F(\theta)$, C_{sca} and C_{sca}^{bb} (Equations (2-3)). The ScattnLay code performs only computations for monosdispere particles. To obtain the phase matrix and cross sections for a polydisperse population, a numerical integration over the size range has to be done off-line (Figure 1, N^{o}S2). A particular attention must be paid to the integration-step size to guarantee the accuracy of the numerical integration.

The Meerhoff Mie program is used to generate a first dataset named DS1 gathering computations of homogeneous spheres for the same study cases as in Twardowski et al. [5]. n_r ranges from 1.02 to 1.2 (with a 0.2 increment), n_i is set to 0.005, D_{min} = 0.012 μm, D_{max} = 152 μm, and ξ is between 2.5 and 5. Note that Twardwoski et al. [5] did not mix different particle components with different refractive indices, as they studied $\widetilde{b_{bp}^{\theta_a}}$ for a polydisperse population of particles having the same refractive index. In this case, Eqs (4)-(6) are not useful as $\widetilde{b_{bp}^{\theta_a}}$ is directly related to $C_{sca}^{bb}/C_{sca}^{\theta_a}$.

In the second dataset (DS2), a distinction is made between VIR, BAC, PHY, DET and MIN in terms of internal structure, refractive index and size range. The scattering properties of phytoplankton cells are modeled using the two-layered sphere model. An exhaustive review of the internal structure of phytoplankton cells was performed by Bernard et al. [22]. They showed that a chloroplast layer (chl) surrounding the cytoplasm (cyt) was an optimal morphology to simulate optical properties of algal cells. Based on their study, the value of the real part of the refractive index for the cytoplasm is fixed to 1.02, and the value of the imaginary part at 532 nm is 1.3357×10^{-4} as calculated from [22]:

$$n_i(cyt, 532\,nm) = n_i(cyt, 400\,nm) \times \exp[-0.01 \times (532 - 400)] \tag{10}$$

with n_i(cyt, 400 nm) = 0.0005. Concerning the chloroplast, n(chl) is calculated according to the Gladstone and Dale formula [31]:

$$\sum_k n_k \times \vartheta_k = n_{equ}, \tag{11}$$

where n_k and ϑ_k are the complex refractive index and the relative volume of the k-th layer, and n_{equ} is the complex equivalent refractive index of the whole particle. The knowledge of the complex equivalent refractive index is useful to compare the simulations of heterogeneous spheres among themselves, regardless the number of layers and the relative proportion of each layer. The complex equivalent refractive index is kept constant (n_{equ}=1.044+i 1.5×10^{-3}). The refractive index of the chloroplast is described in Table 2 according to the relative volume of the chloroplast (20% or 30%). In

Preprints (www.preprints.org) | NOT PEER-REVIEWED | Posted: 2 August 2018 doi:10.20944/preprints201808.0051.v1

Peer-reviewed version available at Appl. Sci. 2018, 8, 2689; doi:10.3390/app8122689

Table 3. Relative abundance of virus (VIR), bacteria (BAC), phytoplakton (PHY), and detritus (DET) with the corresponding bulk refractive index (Equations. 8-9) for the no bloom and no mineral water body (No-B/No-M).

			Relative abundance N^j (%)			
ξ	$\tilde{n_r}$	$\tilde{n_i}$	VIR	BAC	PHY	DET
2.5	1.040	4.067×10^{-4}	78.85	5.374	0.3809	15.39
3	1.041	6.613×10^{-3}	84.74	2.131	8.995×10^{-2}	13.04
4	1.045	8.141×10^{-3}	91.15	0.3193	6.930×10^{-3}	8.528
4.9	1.047	4.759×10^{-3}	94.35	56.74×10^{-3}	7.789×10^{-4}	5.588

DS2, multi-layered sphere models are not implemented for viruses, heterotrophic bacteria, detritus, and minerals because of the paucity of relevant information about their optical and morphometrical properties. As we cannot gather enough accurate information about the internal structure of such particles, the homogeneous sphere model is adopted. The suitable n_r and n_i values for viruses, heterotrophic bacteria, detritus, and minerals are obtained from [23] (Table 1).

4. Abundance of the various particulate components

The relative concentrations N^j associated with each particle group are chosen to realistically represent the mix of marine components and to constrain that the overall size distribution matches with the Junge power law (Tables 3-5 and Figure 2). To compare with typical particulate abundances estimated in natural waters, a total abundance (N_{TOT}) of 1.1262 $\times 10^{14}$ part/m^{-3} is considered as in Stramski et al. [23]. Three study cases are defined. Firstly, a case with no phytoplankton bloom and no mineral particle named No-B/No-M: the phytoplankton abundance (N_{PHY}) spans from 8.8×10^8 (for $\xi = 4.9$) to 4.3×10^{11} part/m^{-3} (for ξ = 2.5) (7.8×10^{-4}% - 0.38% of N_{TOT}). Secondly, a case with a phytoplankton bloom and no mineral (B/No-M), where N_{PHY} is higher as compared to No-B/No-M: N_{PHY} ranges between 6.4×10^9 and 2.0×10^{12} part/m^{-3} (5.7×10^{-3}% - 1.8% of N_{TOT}). Thirdly, a case with minerals and no bloom condition (No-B/M): minerals are added proportionally to obtain a bulk real refractive index $\tilde{n_r}$ around 1.1. The mineral abundance (N_{MIN}) spans from 4.8×10^{12} to 1.3×10^{13} part/m^{-3} (4.2%-11.7% of N_{TOT}). The abundances of the different particle components can be directly compared to the abundances provided in Stramski et al. [23] as N_{TOT} is identical. In Stramski et al. [23], ξ = 4, so comparisons are realized only for this value (Table 6). We note that N_{PHY} is in the same order of magnitude. Stramski et al. [23] selected higher concentrations of DET and MIN and so lower concentrations of VIR and BAC. In their paper, the authors explained that the concentrations of DET and MIN were chosen to obtain a realistic contributions of detrital and mineral absorption. However, to quote one of their sentence, they cautioned against attaching particular significance to their selected DET and MIN concentrations in the context of how well these values can represent realistic concentrations in the ocean. The abundances of viruses and bacteria (N_{VIR} and N_{BAC}), used in this study, are in agreement with Stramki and Kiefer 's values [21]. Stramski and Kiefer [21] (Table 1 in their paper) referenced N_{VIR} between 3.0×10^9 to 4.6×10^{14} part/m^{-3}, N_{BAC} between 3.0×10^{11} to 1.5×10^{12} part/m^{-3}. For phytoplankton, they made a distinction between prochlorophytes, cynobacteria, ultrananoplankton, larger nanoplankton and microplankton. Over this different phytoplankton groups, N_{PHY} ranges between 1.0×10^{11} for picoplankton to 3.0×10^5 for microplankton. They referenced $N_{PHY} \geq 5 \times 10^{11}$ part/m^{-3} when there is bloom of phototrophic picoplankters.

Preprints (www.preprints.org) | NOT PEER-REVIEWED | Posted: 2 August 2018 doi:10.20944/preprints201808.0051.v1

Peer-reviewed version available at Appl. Sci. 2018, 8, 2689; doi:10.3390/app8122689

Table 4. Same as Table 3 but for the water body with phytoplankton bloom conditions and no mineral (B/No-M).

			Relative abundance N^j (%)			
ξ	$\tilde{n}_r$	$\tilde{n}_i$	VIR	BAC	PHY	DET
2.5	1.040	5.820×10^{-4}	51.96	3.939	1.8120	42.29
3	1.041	9.545×10^{-4}	61.91	1.673	0.5407	35.88
4	1.043	1.279×10^{-3}	76.18	0.2757	4.916×10^{-2}	23.49
4.9	1.044	1.017×10^{-3}	84.55	0.0516	5.682×10^{-3}	15.40

Table 5. Same as Table 3 but for waters with minerals and no bloom condition (No-B/M)

			Relative abundance N^j (%)				
ξ	$\tilde{n}_r$	$\tilde{n}_i$	VIR	BAC	PHY	DET	MIN
2.5	1.104	7.297×10^{-4}	70.96	5.311	3.650×10^{-1}	11.68	11.68
3	1.110	8.927×10^{-4}	78.04	2.105	8.801×10^{-2}	9.882	9.882
4	1.132	1.048×10^{-4}	86.75	0.3155	6.902×10^{-3}	6.462	6.462
4.9	1.145	7.403×10^{-6}	91.47	5.607×10^{-2}	7.782×10^{-4}	4.23	4.23

5. Results

5.1. Accuracy of numerical computations

A numerical integration over θ is required to derive $b_p^{\theta_a}$ and b_{bp} from the phase function (section 2-2.3). Due to the sharp increase of the phase function in the forward direction, the selection of the relevant step size for the numerical integration is crucial. For that purpose, the impact of step size ($\Delta\theta$) on the calculation of $\widetilde{b_p^{\theta_a}}$ is studied using Lorentz-Mie simulations in DS1 (Figure 1, N°M2, M3). The scattering function of polydisperse particles exhibits a peak around θ=0° [24]. For small ξ value, that is when the proportion of large-sized particles compared to smaller particles increases, the forward peak is sharper. Indeed, for particles with a large diameter as compared to the wavelength, $F(D,\theta)$ displays a sharp forward peak [24] due the concentration of light near θ=0° caused by diffraction. The presence of this peak requires a number of integration points large enough to provide the desired numerical accuracy. The numerical integration over θ (Figure 1 N°M2) is performed using the "trapz" function from the Numpy package with Python. The "Trapz" function performs an integration along the given axis using the composite trapezoidal rule. To test the accuracy of the integration and to find the correct integration step, $\Delta\theta$, we compare the result of the numerical integration of $F(\theta)$ between 0 and π to its theoretical value (= 2) (Figure 1, N°M3). When $\Delta\theta$ = 0.05, corresponding to a total number of integration steps (N_Θ) of 3600, the numerical integration value of $F(\theta)$ is between [1.999-2.000] for small χ. For larger ξ, it is between [1.800-1.999[. When the value of the numerical integration is between [1.800-1.999[, a renormalization factor is applied to $F(\theta)$ to constraint the value of the numerical integration to be strictly equal to 2. We could also increase the number of integration points but it will increase the computation time. Using a renormalization factor at large ξ is a good compromise to guarantee the accuracy and save computation time.

For two-layered spheres (i.e., phytoplankton cells), the ScattnLay code provides only monodisperse phase functions (Figure 1, N°S1), so the numerical integration over the diameter

Table 6. Comparisons between abundances defined in the present study and abundances defined by Stramski et al. [23]. The hyperbolic slope ξ is 4 and N_{TOT} is 1.1262×10^{14} part/m^{-3}.

	Abundance (part/m^{-3})				
Study case	VIR	BAC	PHY	DET	MIN
No-B/No-M	1.0265×10^{14}	3.5962×10^{11}	7.805×10^{9}	9.6×10^{12}	0
B/No-M	8.5799×10^{13}	3.1047×10^{11}	5.5372×10^{10}	2.6455×10^{13}	0
No-B/M	9.7702×10^{13}	3.5536×10^{11}	7.7733×10^{9}	7.2774×10^{12}	7.2774×10^{9}
Stramski et al. [23]	2.5000×10^{12}	1.0000×10^{11}	2.4759×10^{10}	8.2500×10^{13}	2.7500×10^{13}

(Equation 2) is realized off-line with the python "trapz" function (Figure 1 N^{o}S2). For monodisperse particles, the phase function displays a forward peak as explained above but can also displays a sequence of maxima and minima due to interference and resonance features [24]. The frequency of the maxima and minima over θ increases with both increasing n_r and size parameter (=$\pi\, D/\lambda$). To test the accuracy of the numerical integration over the diameter (Figure 1, N^{o}S3), we run the ScattnLay code for DS1 study cases and compare $F(\theta)$ and C_{sca} rebuilt from Equation (2) with Lorentz-Mie computations as the Lorentz-Mie code provides the polydisperse phase functions and cross section as outputs (Figure 1, N^{o}M1). Note that even a narrow polydispersion washes out the resonance features, explaining why most natural particulate assemblages do not exhibit the resonance patterns [24]. A perfect match is obtained between the ScattnLay-rebuilt-polydisperse and Lorentz-Mie-polydispere $F(\theta)$ and C_{sca} values when the step size (ΔD) is set to 0.01 for D, between [0.03,2[; 0.1 for D between [2,20[; 2.0 for D between [20,200[; 10.0 for D between [200,500].

The impact of the integration on the backscattering ratio $\widetilde{b_{bp}^{\theta_a}}$ is examined from the DS1 data set as a function of the hyperbolic slope ξ for different values of the real refractive index and two number of total integration steps (i.e. 750 and 3600) (Figure 3).The impact of the integration is only noticeable for ξ values lower than about 3 and relatively high n_r values. When the number of integration steps increases, the curves become flatter at low ξ values. Differences in curve shape are reduced if we increase the angle-step size. For $\Delta\theta = 0.24$ (N_Θ=750), the present results of the Lorentz-Mie calculations (solid lines in Figure 3) perfectly match those previously obtained by Twardowski et al. [5] (not shown). However, in this case (N_Θ=750), the numerical integration is not accurate enough as the integration of Equation (1) gives values between 1.999 (ξ=4.9) and 1.04 ($\xi = 2.5$). In the following, $\Delta\theta$ is set to 0.05 (N_θ=3600), and Figure 3 (dashed lines) will be the reference figure for homogeneous spheres.

5.2. Impact of the heterogeneity of phytoplankton cells on the bulk particulate backscattering ratio

The impact of phytoplankton heterogeneity on $\widetilde{b_{bp}^{\theta_a}}$ is examined as a function of ξ for the three previously described water bodies (No-B/No-M, B-No-M, No-B/M) considering the 80%-20% phytoplankton morphological model (Figure 4a). This impact is evaluated by comparison with Lorentz-Mie calculations (homogeneous spheres) performed for low (phytoplankton-dominated, Case 1 water), and high (mineral-dominated, Case 2 water) refractive index. The real and imaginary part values of the refractive index are 1.0458 and 0.0007, for the "Ref. Case 1" study case, and 1.138 and 3.85×10^{-5} for the "Ref. Case 2" study case, respectively (Figure 4b,c). In contrast to these two reference water bodies, the real and imaginary bulk refractive index for No-B/No-M, B-No-M and No-B/M, vary with ξ as the relative proportions of the different particle components, having different n_r and n_i, vary with ξ (Tables 1-2 and Tables 3-5). For the no-mineral water bodies (No-B/No-M and B/No-M), $\tilde{n}_r$ stays around 1.04$\pm$0.007 (Figure 4b). In contrast, $\tilde{n}_i$ shows large variation with ξ for both No-B/No-M and B/No-M water bodies (Figure 4c). In bloom conditions, $\tilde{n}_i$ increases as the relative

proportion of phytoplankton increases as compared to the no bloom conditions. In agreement with the typical oceanic bulk n_i values [32], the $\tilde{n}_i$ values for the particulate populations considered here are always lower than 0.002. In presence of mineral particles (No-B/M), $\tilde{n}_r$ increases as MIN have a higher n_r than VIR, BAC, PHY and DET. Its values are between 1.10 ($\xi = 2.5$) and 1.14 ($\xi = 4.9$). Values of $\tilde{n}_i$ vary between 7.4×10^{-6} and 8.9×10^{-4}.

The impact of heterogeneity on the particulate backscattering ratio can only be discussed when the $\tilde{n}_i$ and $\tilde{n}_r$ values are equal to those fixed for the homogeneous models. Because of the strong variation of $\tilde{n}_i$ with ξ for the three considered water bodies (No-B/No-M, B/No-M, and No-B/M), this condition is satisfied only for $\xi = 4.3$ (i) between No-B/No-M and Ref. Case 1 (ii) between No-B/M and Ref. Case 2. The variation of $\widetilde{b_{bp}^{\theta_a}}$ due to heterogeneity of phytoplankton cells is evaluated using the relative difference (in absolute value) calculated between the homogeneous and heterogeneous cases.

Even if the relative proportion of phytoplankton is very small for the No-B/No-M water body(=3.329×10^{-3}%), the heterogeneity increases the $\widetilde{b_{bp}^{\theta_a}}$ value by 60% compared to the homogeneous case (Ref. Case 1) with the same value of refractive index. This is coherent with previous studies showing the great contribution of coated spheres to the backscattering signal [13,14], [16,17], [20], [33]. The value of the relative difference calculated between the No-B/No-M and B/No-M water bodies is smaller (=27%) even if $\tilde{n}_i$ is different (0.0007 for No-B/No-M against 0.0012 for B-No-M). This latter pattern evidences that the heterogeneity (coated-sphere model) has a greater impact on the particulate backscattering ratio than an increase in the bulk imaginary refractive index.

The impact of the relative volume of the cytoplasm on $\widetilde{b_{bp}^{\theta_a}}$ is now evaluated by comparing the evolution of $\widetilde{b_{bp}^{\theta_a}}$ as a function of ξ for the 80%-20% and 70%-30% models for the No-B/No-M and B/No-M water bodies (Figure 5). The mean relative difference on $\widetilde{b_{bp}^{\theta_a}}$ is about 4% with a maximum value of 8.5 % for No-B/No-M. In bloom conditions, the mean relative difference reaches 10% with a maximum value of 20%. This relatively weak impact of the morphological model on $\widetilde{b_{bp}^{\theta_a}}$ is explained by the relatively constant values of $\tilde{n}_r$ and $\tilde{n}_i$ for the two models (the differences are less than 1×10^{-5} for $\tilde{n}_r$ and 3.5×10^{-5} for $\tilde{n}_i$). These latter small differences of the refractive index between the two models are due to the fact that the real and imaginary part of the phytoplankton equivalent refractive index are identical for the 80%-20% and 70%-30% models and differences on C_{sca}^{PHY} between 80%-20% and 70%-30% are not important enough to impact significantly $\tilde{n}_r$ and $\tilde{n}_i$ as they are weighted by a weak phytoplankton relative abundance.

When mineral particles are taken into account, the impact of heterogeneity can be examined for a ξ value of 4.3, where the real and imaginary parts of the refractive index are similar between the homogeneous case (Ref. Case 2) and the heterogeneous case (No-B/M), ($\tilde{n}_r$=1.137 and $\tilde{n}_i$=3.85×10^{-5}). For this specific case, the $\widetilde{b_{bp}^{\theta_a}}$ value increases only by 6% between the homogeneous and heterogeneous cases, both in presence of mineral particles. This weak difference is due to the fact that phytoplankton has a smaller impact on the bulk scattering when highly scattering particles like minerals are added.

6. Concluding remarks

We show in the present study that a special care should be taken in the integration step size when the particulate scattering coefficients are calculated from the particulate scattering function, especially for relatively low PSD slope. We show that an integration step size of 0.05 (N_Θ=3600) is required to obtain the required accuracy considering the inputs (refractive indices and size range) used in this study.

Modeling phytoplankton cells as two-layered spheres tends to increase the bulk backscattering ratio because heterogeneous spheres are more efficient backscatterers. Even if the phytoplankton component has the weakest relative abundance, its impact on $\widetilde{b_{bp}^{\theta_a}}$ can be important depending on the

hyperbolic slope of the Junge distribution. For $\xi = 4.3$, the relative difference (in absolute value), (ΔE), can reach about 60% between $\widetilde{b_{bp}^{\theta_a}}$ for No-B/No-M and the reference case, having the same bulk refractive index but composed exclusively of homogeneous spheres. When minerals are added, the impact of phytoplankton decreases as the scattering by minerals dominates.

Considering different sub-populations of particles with different refractive indices involves that the bulk refractive index varies with the value of the hyperbolic slope. It results that the development of semi-analytical relationships to derive $\tilde{n}_r$ from $\widetilde{b_{bp}^{\theta_a}}$ and ξ, is not straightforward. Semi-analytical relationships, such as the one developed by Twardowski et al. [5], may be replaced by an approach using look-up tables.

In this study, a large set of numerical simulations, as well as a proper methodology have been developed to rebuild the particulate scattering properties of a water body in its complexity. This method is adapted to be used repeatedly to model a very large variety of particulate assemblages. While, the present study has been limited to three study cases, additional calculations should be carrying out to be able to better represent the variability encountered in oceanic environments in terms of particulate community and its complexity in terms of mixing, morphology, size, and chemical nature.

Further work is required, mainly from experimental studies, to better characterize the internal structure and chemical composition of viruses, heterotrophic bacteria, biogenic detritus, and aggregates. This will allow, as Bernard et al. [22] did for phytoplankton, suitable models to be developed, to describe properly, in numerical code, the morphological properties of such particles in order to provide more realistic simulations of their optical properties.

Acknowledgments: The authors gratefully acknowledge the support from the French Space Agency (CNES) through the COYOTE project (CNES/TOSCA program). The authors thank Prof. Michael Twardowski, (Harbor Branch Oceanographic Institute) for the precious advices. Experiments presented in this paper were carried out using the CALCULCO computing platform, supported by SCoSI/ULCO (Service COmmun du Système d'Information de l'Université du Littoral Côte d'Opale).

Conflicts of Interest: The authors declare no conflict of interest

References

1. Preisendorfer, R.W. Hydrologic optics, Vol.1: Introduction, *Springfield National Technical Information Service, Office of Naval Research*, **1976**.
2. Morel, A. The scattering of light by seawater: experimental results and theoretical approach. *Translation by George Halikas of the paper published in French in AGARD Lecture Series*, **1976**, N°61 (1973).
3. Boss, E.; Pegau, W.S.; Gardner, W.D.; Zaneveld, J.R.V.; Barnard, A.H.; Twardowski, M.S.; Chang, G.C.; Dickey, T.D. The spectral particulate attenuation and particle size distribution in the bottom boundary layer of a continental shelf", *J. Geophys. Res.*, **2001**, *106(C5)*, 9509-9516.
4. Boss, E.; Twardowski, M.S.; Herring, S. Shape of the particulate beam attenuation spectrum and its relation to the size distribution of oceanic particles. *Appl. Opt.*, **2001**, *40*, 4885-4893.
5. Twardowski, M.; Boss, E.; Macdonald, J.; Pegau, W.; Barnard, A.; Zaneveld, J. A model for estimating bulk refractive index from optical backscattering ratio and the implications for understanding particle composition in case I and case II waters, . *J. Geophys. Res.*, **2001** *106(C7)*, 14,129–14,142.
6. Boss, E.; Pegau, W.S.; Lee, M.; Twardowski, M.; Shybanov, E.; Korotaev, G.; Baratange, F. Particulate backscattering ratio at LEO 15 and its use to study particle composition and distribution, *J. Geophys. Res.* **2004**, *109*, *C01014*, doi:10.1029/2002JC001514.
7. Loisel, H.; Mériaux, X.; Berthon, J.F.; Poteau A. Investigation of the optical backscattering to scattering ratio of marine particles in relation to their biogeochemical composition in the eastern English Channel and southern North Sea, *Limnol. Oceanogr.*, **2007**, *52(2)*, 739–752.
8. Nasiha, H.J.; Shanmugam, P. Estimating the Bulk Refractive Index and Related Particulate Properties of Natural Waters From Remote-Sensing Data, *IEEE J. Sel. Top. Appl. Earth Obs. Remote Sens.*, **2015**, *8 (11)*, 5324-5335, doi: 10.1109/JSTARS.2015.2439581.

9. Snyder, W.A.; Arnone, R. A.; Davis, C. O.; Goode, W.; Gould, R. W.; Ladner, S.; Lamela, G.; Rhea, W. J.; Stavn, R., Sydor, M.; Weidemann, A. Optical scattering and backscattering by organic and inorganic particulates in U.S. coastal waters, *Appl. Opt.*, **2008**, 47, 666-677, doi.org/10.1364/AO.47.000666
10. Sullivan, J.; Twardowski,M.; Donaghay, P.; Freeman, S. Use of optical scattering to discriminate particle types in coastal waters, *Appl. Opt.*, **2005**, 44, 1667-1680, https://doi.org/10.1364/AO.44.001667
11. Bricaud, A; Zaneveld, J.R.V; Kitchen, J.C. Backscattering efficiency of coccolithophorids: use of a three-layered sphere model, *Proc. SPIE.*, **1992**, *1750*, 27–33.
12. Kitchen, J.C.; Zaneveld, J.R.V. A three-layered sphere model of the optical properties of phytoplankton, *Limnol. Oceanogr.*, **1992**, *37(8)*, 1680–1690, doi.org/10.4319/lo,.1992.37.8.1680.
13. Moutier, W.; Duforêt-Gaurier, L.; Thyssen, M.; Loisel, H.; Mériaux, X.; Courcot, L.; Dessailly, D.; Rêve, A. H.; Grégori, G. Alvain, S.; Barani, A.; Brutier, L.; Dugenne, M. Evolution of the scattering properties of phytoplankton cells from flow cytometry measurements, *PLoS ONE*, **2018**, *12(7)*, doi.org/10.1371/journal.pone.0181180.
14. Poulin, C.; Zhang, X.; Yang, P.; Huot, Y. Diel variations of the attenuation, backscattering and absorption coefficients of four phytoplankton species and comparison with spherical, coated spherical and hexahedral particle optical models, *J. Quant. Spectros. and Radiat. Transf.*, **2018**, *217*, 288-304, doi.org/10.1016/j.jqsrt.2018.05.035.
15. Quirantes, A.; Bernard, S. Light scattering by marine algae: two-layer spherical and nonspherical models, *J. Quant. Spectros. and Radiat. Transf.*, **2004**, *89*, 311-321, doi.org/10.1016/j.jqsrt.2004.05.031.
16. Vaillancourt, R.D.; Brown, C.W. ; Guillard, R.L. ; Balch, W.M. Light backscattering properties of marine phytoplankton: relationships to cell size, chemical composition and taxonomy, *J. Plankton Res.*, **2004**, *26(2)*, 191-212. doi.org/10.1093/plankt/fbh012.
17. Volten, H. ; Haan, J.F.; Hovenier, J.W.; Schreurs, R.; Vassen, W.; Dekker, A.G.; Hoogenboom, H.J; Charlton, F.; Wouts, R. Laboratory measurements of angular distributions of light scattered by phytoplankton and silt, *Limnol. Oceanogr.*, **1998**, *43(6)*, 1180-1197, doi.org/10.4319/lo.1998.43.6.1180.
18. Witkowski, K.; Król, T.; Zielinski, A.; Kuten, E. A light-scattering matrix for unicellular marine phytoplankton, *Limnol. Oceanogr.*, **1998**, *43(5)*, 859–869, doi.org/10.4319/lo.
19. D. Stramski, E. Boss, D. Bogucki, K. J. Voss, "The role of seawater constituents in light backscattering in the ocean", *Prog. Oceanogr.*, **61**, 27-56, (2004).
20. Whitmire, A.L.; Pegau, W.S.; Karp-Boss, L.; Boss, E.; Cowles, T.J. Spectral backscattering properties of marine phytoplakton cultures, *Opt. Express*, **2010**, *18(14)*, 15073-15093.
21. Stramski, D.; Kiefer, D.A. Light scattering by microorganisms in the open ocean, *Prog. Oceanogr.*, **1991**, *28(4)*, 343-383.
22. Bernard, S.; Probyn T.A.; Quirantes A. Simulating the optical properties of phytoplankton cells using a two-layered spherical geometry. *Biogeosciences*, **2009**, 1497-1563.
23. Stramski, D.; Bricaud, A.; Morel, A. Modeling the inherent optical properties of the ocean based on the detailed composition of the planktonic community, *Appl. Opt.*, **2001** *40(18)*, 2929-2945.
24. Mishchenko, M.I.; Travis, L.D.; Lacis, A.A., *Scattering, Absorption and Emission of Light of Small Particles*, Cambridge University Press, **2002**.
25. Jonasz, M. Particle size distribution in the Baltic, *Tellus*, **1983**, B35, 346-358.
26. Loisel, H., Nicolas; J.M.; Sciandra, A.; Stramski, D.; Poteau A., Spectral dependency of optical backscattering by marine particles from satellite remote sensing of the global ocean, *J. Geophys. Res.*, **2006**, 111, C09024, doi:10.1029/2005JC003367.
27. Boss, E.; Slade, W. H.; Behrenfeld, M.; Dall'Olmo, G. Acceptance angle effects on the beam attenuation in the ocean, *Opt. Express*, **2009**, *17*, *3*, doi.org/10.1364/OE.17.001535.
28. Dolman, V.L. Meerhoff Mie Program User Guide,*Internal Report Astronomy Dept.*, Free University, **1989**.
29. Peña, O.; Pal, U. Scattering of electromagnetic radiation by a multilayered sphere. *Computer Physics Communications*, **2009**, *180(11)*, 2348-2354, doi.org/10.1016/j.cpc.2009.07.010.
30. Yang W., Improved recursive algorithm for light scattering by a multilayered sphere, *Appl. Opt.*, **2003**, *42(9)*, 1710-1720.
31. Aas, E. Refractive index of phytoplankton derived from its metabolite composition. *J. Plankton Res.* **1996** *18*(12), 2223–2249, doi.org/10.1093/plankt/18.12.2223.

32. Bricaud, A.; Roesler, C.; Zaneveld, J.R.V. In situ methods for measuring the inherent optical properties of ocean waters, *Limnol. Oceanogr.*, **1995**, *40*, 393-410.
33. Zaneveld, J.R.V.; Kitchen, J.C. The variation in the inherent optical properties of phytoplankton near an absorption peak as determined by various models of cell structure, *J. Geophys. Res.*, **1995**, *100(C7)*, 309-313, doi.org/10.1029/95JC00451

Preprints (www.preprints.org) | NOT PEER-REVIEWED | Posted: 2 August 2018 doi:10.20944/preprints201808.0051.v1

Peer-reviewed version available at Appl. Sci. 2018, 8, 2689; doi:10.3390/app8122689

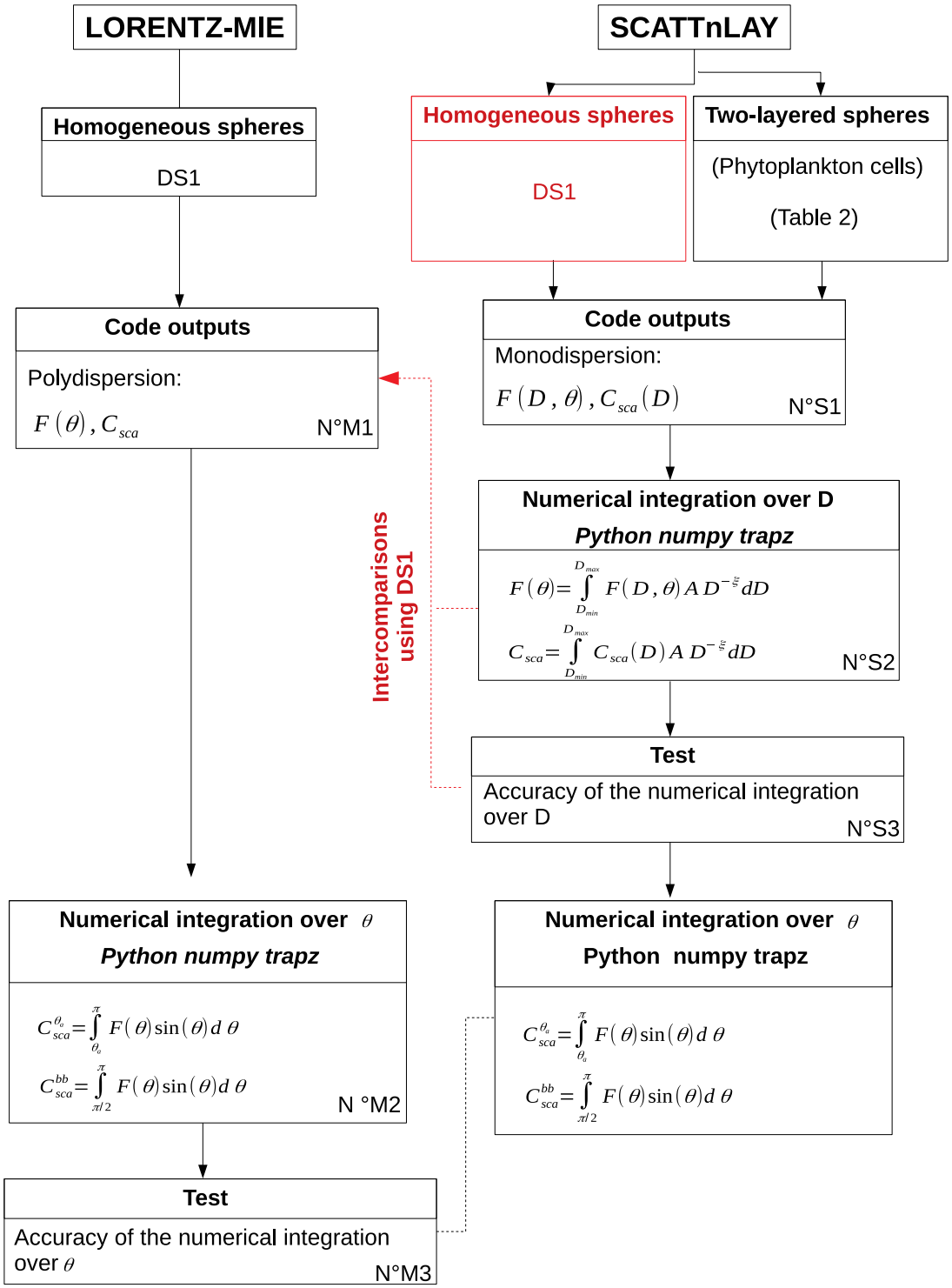

Figure 1. Flow chart of the integration procedure applied to the MIE and ScattnLay outputs.

Preprints (www.preprints.org) | NOT PEER-REVIEWED | Posted: 2 August 2018 doi:10.20944/preprints201808.0051.v1

Peer-reviewed version available at Appl. Sci. 2018, 8, 2689; doi:10.3390/app8122689

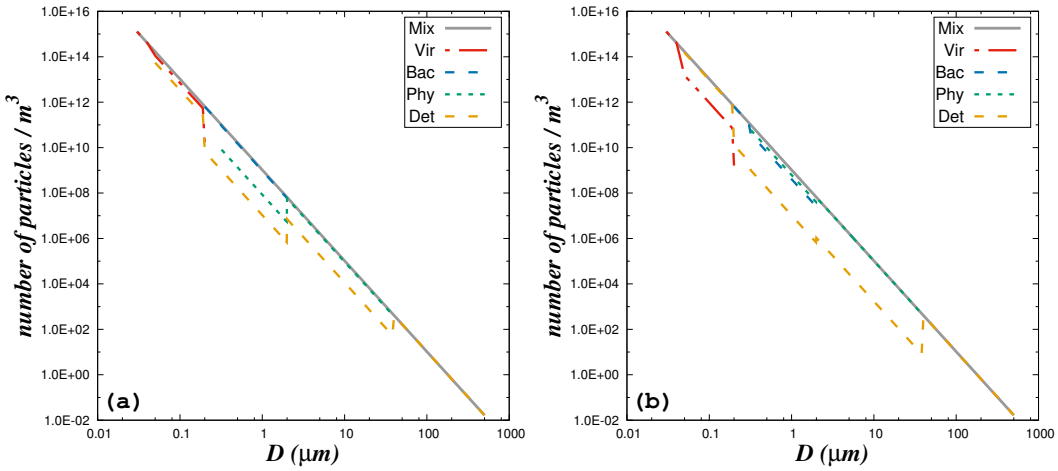

Figure 2. Composite PSD as derived from individual PSD of the five considered particle groups for (a) the no bloom and no mineral particle water body (No-B/No-M) and (b) bloom situation with no mineral particle (B/No-M). N_{TOT} = 1.1262 $\times 10^{14}$ par/m^{-3} and ξ = 4.

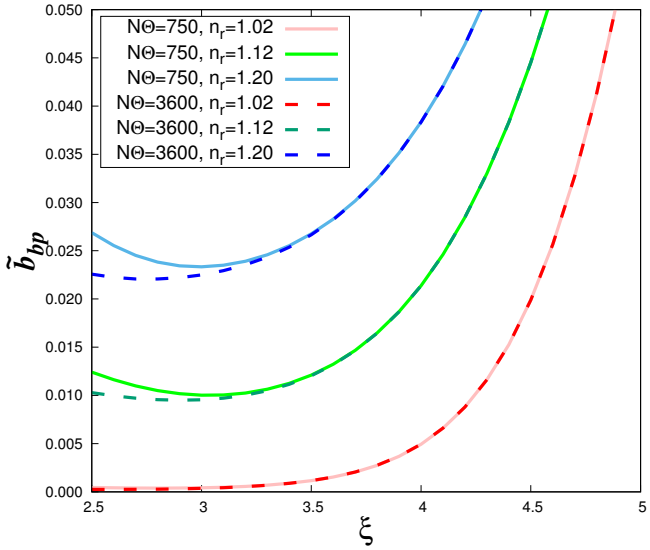

Figure 3. Results of Lorentz-Mie calculation (DS1) of the particulate backscattering ratio $\widetilde{b_{bp}^{\theta_a}}$ as a function of the hyperbolic slope, ξ, and different values of n_r and N_Θ. The imaginary part of the refractive index = 0.005 as in Twardowski et al. [5]. This figure can be compared to Figure 1 in Twardowski et al. [5].

Peer-reviewed version available at Appl. Sci. 2018, 8, 2689; doi:10.3390/app8122689

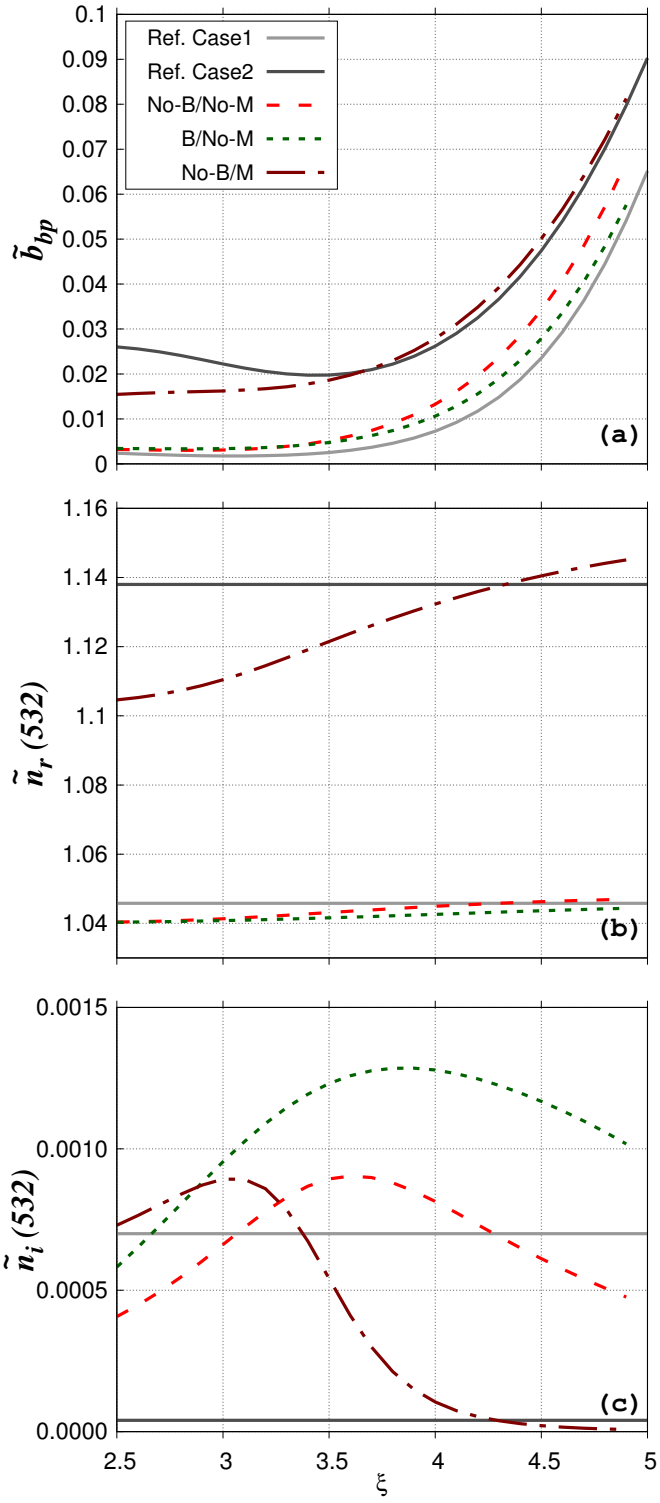

Figure 4. (a) Particulate backscattering ratio $\widetilde{b_{bp}^{\theta_a}}$ as a function of the hyperbolic slope for the No-B/no-M (red dashed line), B/No-M (green dashed line), and No-B/M (brown dashed line) water bodies as referenced in section 4. Black and gray lines are for homogeneous spheres with n_r = 1.0458, n_i = 0.0007 and n_r = 1.138, n_i = 3.85×10^{-5}, respectively. Phytoplankton cells are modeled as two-layered spheres with a relative volume of the cytoplasm of 20 % (%cyt-%chl)=80-20). (b) as in panel (a) but for the real refractive index. (c) as in panel (a) but for the imaginary part of the refractive index.

Peer-reviewed version available at Appl. Sci. 2018, 8, 2689; doi:10.3390/app8122689

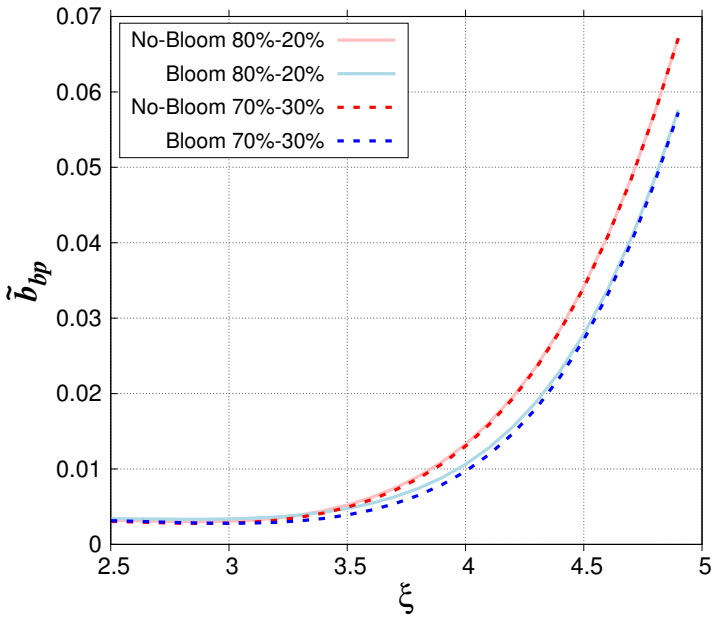

Figure 5. Particulate backscattering ratio as a function of the hyperbolic slope for No-B/no-M and B/No-M water bodies conditions. Phytoplankton cells are modeled as two-layered spheres with a relative volume of the cytoplasm of 20 % and 30 %, as indicated.